Evaporation of Water Nanodroplets on Heated Surfaces: Does Nano Matter?

Luis Ruiz Pestana[1*], Teresa Head-Gordon[2]

[1]*Department of Civil and Architectural Engineering, University of Miami, Coral Gables, FL 33146, USA*
[2]*Department of Chemistry, Bioengineering, and Chemical and Biomolecular Engineering, University of California, Berkeley, and Chemical Sciences Division, Lawrence Berkeley National Laboratory, CA 94720, USA*

ABSTRACT

While experiments and continuum models have provided a relatively good understanding of the evaporation of macroscopic water droplets, elucidating how sessile nanodroplets evaporate is an open question critical for advancing nanotechnological applications where nanodroplets can play an essential role. Here, using molecular dynamics simulations, we find that evaporating nanodroplets, in contrast to their macroscopic counterparts, are not always in thermal equilibrium with the substrate and that the vapor concentration on the nanodroplet surface does not reach a steady state. As a result, the evaporative behavior of nanodroplets is significantly different. Regardless of hydrophobicity, nanodroplets do not follow conventional evaporation modes, but instead exhibit dynamic wetting behavior characterized by huge, non-equilibrium, isovolumetric fluctuations in the contact angle and contact radius. For hydrophilic nanodroplets, the evaporation rate, controlled by the vapor concentration, decays exponentially over time. Hydrophobic nanodroplets follow stretched exponential kinetics arising from the slower thermalization with the substrate. The evaporative half-lifetime of the nanodroplets is directly related to the thermalization time scale and therefore increases monotonically with the hydrophobicity of the substrate. Finally, the evaporative flux profile along the nanodroplet surface is highly non-uniform but does not diverge at the contact line as the macroscopic continuum models predict.

*Corresponding author: luisruizpestana@miami.edu

Keywords: nanodroplet, water, evaporation, molecular dynamics, kinetics, non-equilibrium.

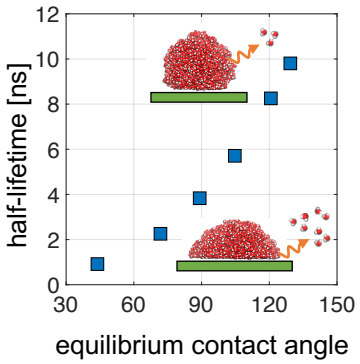

Table of Content (TOC) Figure.

Understanding the wetting behavior and evaporation kinetics of droplets on solid substrates (i.e., sessile droplets) is of great importance to many engineering and technological applications such as inkjet printing,[1] nanofabrication,[2] biochemical assays,[3] or evaporative cooling of electronics.[4, 5] The evaporation of macroscopic droplets has been extensively studied,[6-9] and theoretical models exist that, assuming the evaporation mode, can predict the evaporation kinetics relatively well.[10-12] Depending on how the contact radius R and contact angle θ evolve over time, two pure modes of evaporation, the constant contact angle (CCA) and the constant contact radius (CCR) modes, have been recognized and experimentally observed for macroscopic droplets. Under quasi-equilibrium ideal conditions, the CCA mode is expected as the contact angle takes a unique value determined by Young's equation.[13] Evaporation in CCR mode requires pinning of the contact line, which can only occur in the presence of surface roughness or chemical heterogeneities in the substrate that affect the balance of surface tensions at the vapor-liquid-solid interface. For droplets on heterogeneous substrates, mixed modes of evaporation, such stick-slip motion of the contact line, have also been observed.[14, 15] Since the pioneer work by Picknett and Bexon[16] leading to the well-known d^2-law, where the droplet contact area on the substrate decreases linearly with time, the evaporation of sessile droplets has been modeled as a process limited by the diffusive relaxation of the saturated vapor outside the liquid-vapor interface. Another assumption of the model is the steady state of the vapor concentration field, which is valid when the time scale of the evaporation is much longer than the time scale associated to the diffusive dissipation of the vapor. In two seminal papers, Deegan et *al.*[17, 18] showed that the diffusion-limited model of evaporation predicts, for hydrophilic sessile droplets evaporating in CCR mode, the divergence of the evaporative flux at the contact line, $J(r) \propto (R-r)^{-\lambda}$, where R is the contact radius, r is the distance from the axisymmetric axis of the droplet to the surface, and the exponent λ is a function of the contact angle.[19] A direct consequence of the non-uniform flux and the pinned contact line is the flow of fluid from the interior of the droplet to replenish the contact line, which explains the puzzling ring-like stains left by evaporated coffee drops. For hydrophobic droplets, the diffusion-limited model predicts zero flux at the contact line, which gradually increases from the contact line towards the maximum diameter of the droplet, and then remains approximately constant towards the cusp.[20, 21] For a droplet with a contact angle of 90°, the theoretical prediction is a completely uniform evaporative flux along the droplet surface.

A similar level of understanding of the evaporation mode, kinetics, and evaporative flux is lacking at the nanoscale, where many of the assumptions of the continuum models break down and systems become extremely challenging to probe experimentally. In the last decade or so, molecular dynamics (MD) simulations, which do not rely on the major simplifying assumptions of the continuum models, have been used to gain insight into the evaporation and wetting behavior of water at the molecular level. Previous work on the evaporation of water at the molecular and nanoscale level has been primarily focused on the wetting behavior of sessile nanodroplets as a function of size and temperature,[22, 23] on the evaporation of films[24-26] and free-standing nanodroplets,[27, 28] and on the quantification of accommodation coefficients, which still remains a controversial issue.[29, 30] Simulations of sessile nanodroplets have shed some light into the role of hydrophobicity on the evaporative behavior,[31-34] however prior studies have overwhelmingly focused on simple Lennard-Jones fluids, thus offering limited insight into the behavior of water nanodroplets, mediated by directional interactions such as hydrogen bonds. To the best of our knowledge, only Reese and co-workers have simulated the evaporation of pure sessile water nanodroplets,[35] which they found to evaporate in CCR mode on platinum surfaces. In that study, the mechanism underlying the pinning of the contact line in the ideal platinum substrate is unclear, and only hydrophilic nanodroplets were investigated. Many fundamental questions remain regarding the evaporative behavior of water sessile nanodroplets and whether conventional macroscopic models can be applied.

In this paper we use molecular dynamics simulations of water nanodroplets on heated substrates with different hydrophobicity to study the evaporative behavior of water sessile nanodroplets and compare our results to the predictions of macroscopic models. As a function of hydrophobicity, we characterize the evaporation mode and the large fluctuations in contact angle and contact radius during evaporation, quantify and model the evaporation kinetics, and map the evaporative flux profile along the liquid-vapor interface of the nanodroplet. For the latter, we perform an ensemble analysis of the trajectories of single molecules that offers a clear view of the evaporative flux profile which, stemming from the large fluctuations and the rapidly evolving geometry of the nanodroplets, has been notoriously difficult to calculate and thus avoided in previous studies.

RESULTS AND DISCUSSION

Here, we simulate the evaporation of sessile nanodroplets containing 2,749 water molecules (~3 nm radius) adsorbed to a non-chemically specific substrate that is ~1 nm thick. The simulation box dimensions are ~14 x 14 x 15 nm^3, and we simulate the evaporation of nanodroplets with a wide range of contact angles, from 45° to 130°. All the nanodroplets are first equilibrated on the substrate at 300 K for 20 ns. At the end of the equilibration stage, before heating up the substrate to promote evaporation, the nanodroplet is in equilibrium with its vapor and adopts an equilibrium contact angle. Once the systems are equilibrated, we instantaneously increase the temperature of the substrate to 520 K to promote evaporation, which is commensurate with temperatures previously used in simulation studies[30, 35] as well as experiments on the evaporation of microscopic droplets on superheated substrates.[36] The dynamics of the substrate atoms are integrated in the NVT ensemble, and those of the water molecules in the NVE ensemble to avoid introducing artifacts in their dynamics. Similar simulation protocols have been widely applied to simulate the evaporation of nanodroplets.[35, 37] In our setup, the substrate temperature is maintained constant during the evaporation process, which mimics a situation where the substrate would be much more massive than the nanodroplet, which we believe will be the case in most applications. We decided not to impose boundary conditions where the heat flux between the substrate and the nanodroplet is maintained constant because those conditions are less experimentally relevant in the context of nanodroplet evaporation. Further methodological details about the MD simulations conducted for this study are provided in the Methods section. In the following sections we show our results on the evaporative behavior of sessile nanodroplets and discuss how it differs from the evaporation of macroscopic droplets.

Dynamic wetting behavior. In our simulations, the substrate is chemically homogeneous and atomically smooth, thus we don't expect (and don't observe) pinning of the contact line, which rules out at the outset the possibility of evaporating in CCR mode. Figure 1 shows the evolution of the contact angle, R, and contact radius, θ, during evaporation. We find that R steadily decreases during evaporation for all the cases studied here, regardless of the hydrophobicity of the substrate. Except for the nanodroplet with $\theta_{\mathrm{eq}} = 90^{o}$, where θ remains approximately constant during evaporation (Figure 1D), the nanodroplets do not follow the CCA mode either. Interestingly, how θ evolves over time depends strongly on the hydrophobicity of the substrate. For all the hydrophobic cases the contact angle significantly increases during evaporation, which implies that hydrophobic nanodroplets become more hydrophobic as they evaporate (Figure 1A-C). In the two

most hydrophobic cases, the dynamic dewetting process goes as far as to completely desorb the nanodroplet from the substrate before it fully evaporates (Figure 1A-B). The states when the nanodroplets were detached from the substrate are illustrated by darker orange and green points in in Figure 1A and 1B, respectively. For purely illustrative purposes, as neither θ or R are well defined when the nanodroplet is desorbed, we assign θ a value of 180^o and make R equal to the radius of the sphere that fits the suspended nanodroplet. The hydrophilic nanodroplets also exhibit dynamic wetting behavior, which is particularly clear for the more hydrophilic case (Figure 1F). However, the change in θ is in the opposite direction than for the hydrophobic ones, i.e., hydrophilic nanodroplets become more hydrophilic as evaporation progresses (Figure 1E-F).

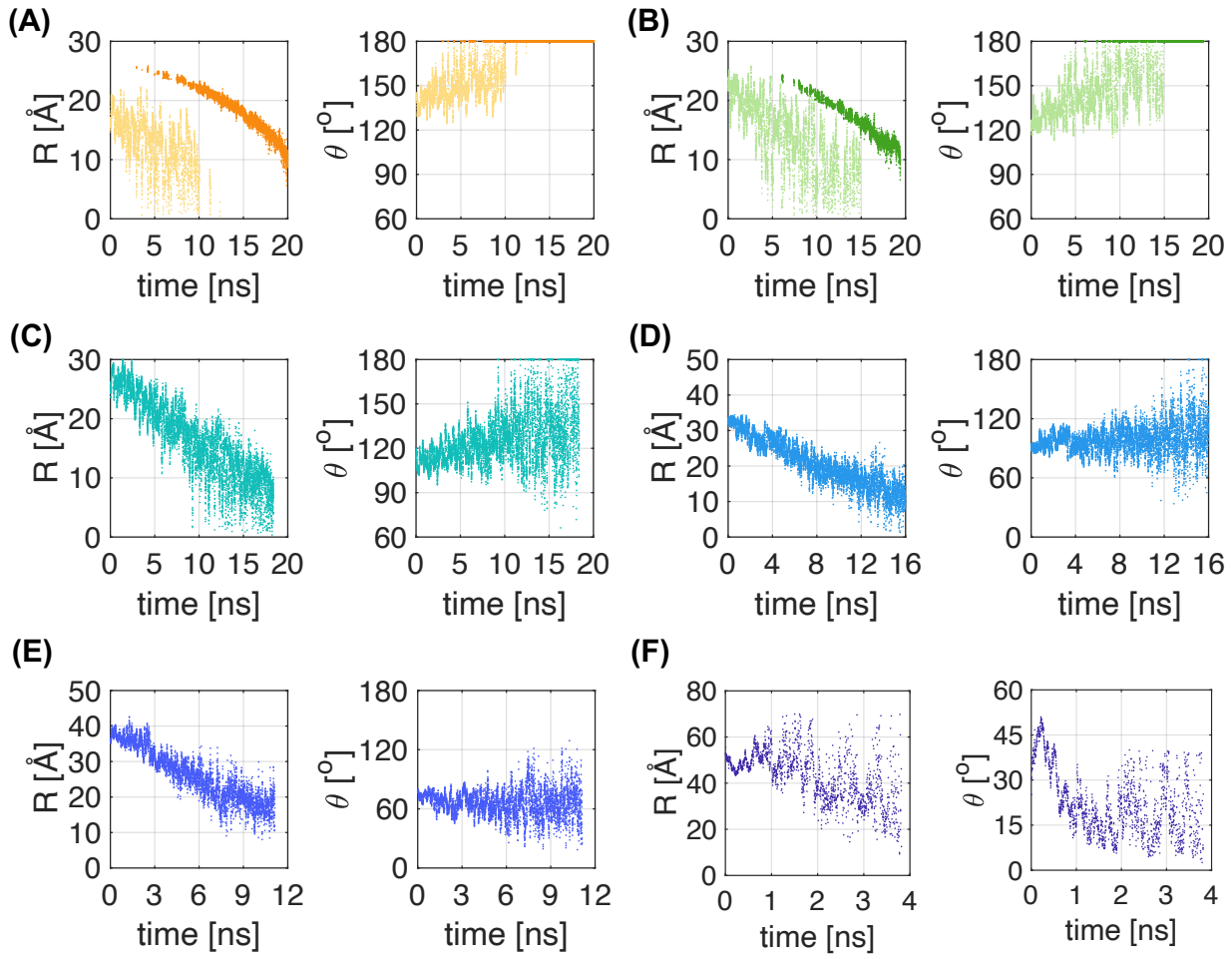

Figure 1. Evolution of the contact radius, R, and contact angle, θ, during evaporation. Each panel corresponds to a case with different hydrophobicity: (A) $\theta_{eq} = 130^o$, (B) $\theta_{eq} = 120^o$, (C) $\theta_{eq} = 105^o$, (D) $\theta_{eq} = 90^o$, (E) $\theta_{eq} = 70^o$, (F) $\theta_{eq} = 45^o$. The darker yellow and green points in panels (A) and (B) indicate states where the nanodroplet is suspended (i.e., desorbed from the substrate). As neither θ or R are

well defined when the nanodroplet is suspended, we assign θ a value of 180^o, and make R equal to the radius of the sphere that fits the suspended nanodroplet.

The dynamic wetting behavior that we observe could be caused by size or thermal effects. During evaporation, the temperature of the nanodroplet increases from room temperature to thermalize with the heated substrate, and its size decreases as water molecules transfer from the liquid into the vapor phase. In the case of macroscopic water droplets, the droplet size has no effect on the wetting properties, but the contact angle has been observed to decrease as a function of temperature on hydrophilic surfaces,[38] and overall to remain constant on hydrophobic substrates.[39] To address whether the same phenomenology applies to the evaporating nanodroplets, we carried out a set of equilibrium simulations of nanodroplets of three different sizes, on four substrates with different hydrophobicity, and at three different temperatures. The results of those simulations, shown in Figure 2, indicate that the temperature of the substrate affects the equilibrium contact angle more strongly than the size of the nanodroplet, and produces the opposite effect in hydrophobic and hydrophilic cases, with hydrophobic droplets becoming more hydrophobic, and hydrophilic ones becoming more hydrophilic (Figure 2A). Increasing the droplet size only results in modest increases in the contact angle independently of the substrate hydrophobicity (Figure 2B). The trends shown in Figure 3 are consistent with the dynamic wetting behavior observed during the evaporation process.

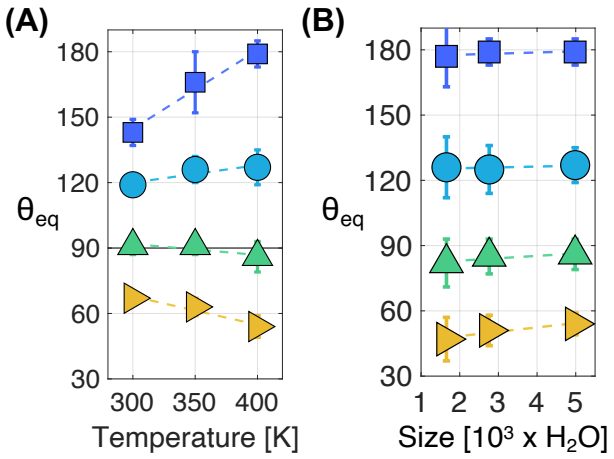

Figure 2. Temperature and size effects on the equilibrium contact angle of the nanodroplets. (A) Equilibrium contact angle as a function of temperature. The data shown corresponds to the nanodroplet containing 4,985 water molecules, the largest studied, but similar trends are observed for the other sizes. (B) Equilibrium contact angle as a function of nanodroplet size in number of water molecules. The data shown corresponds to a temperature of 400 K, but the other cases at 300 and 350 K also show similar trends.

Large non-equilibrium, isovolumetric fluctuations. A salient feature in the plots shown in Figure 3, is that both R and θ display very large fluctuations with respect to their moving averages. These fluctuations have been generally ignored even in studies of nanoscale droplets, where smoothed moving averages are typically reported.[32, 33, 37, 40] For a system in equilibrium, the relative fluctuations, $\Delta = \sigma/\mu$, where μ is the mean and σ is the standard deviation, in energy, density, and other thermodynamic quantities, scale with the size of the system as $\Delta \propto 1/\sqrt{N}$. Accordingly, we expect the relative fluctuations in contact radius and contact angle to become larger as the nanodroplet decreases in size during evaporation, which is what we observe (Figure 3). However, the scaling of the fluctuations in the contact angle, Δ_θ, plotted as a function of the instantaneous size of the nanodroplet, reveals that $\Delta_\theta \propto 1/N$, which reveals the non-equilibrium nature of the fluctuations. The N^{-1} scaling leads to much larger fluctuations as the nanodroplet evaporates and decreases in size than those expected if the nanodroplet were in equilibrium during the evaporation (which is a typical assumption of the macroscopic continuum methods). The scaling with nanodroplet size of the fluctuations in R, although not shown in the figure, are analogous.

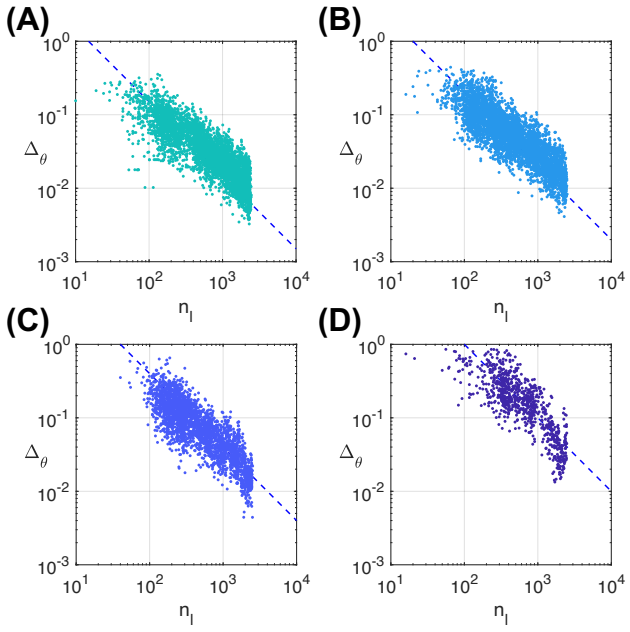

Figure 3. Scaling of the fluctuations of the contact angle Δ_θ with the instantaneous size of the nanodroplet n_l. (A) $\theta_{eq} = 105^o$, (B) $\theta_{eq} = 90^o$, (C) $\theta_{eq} = 70^o$, (D) $\theta_{eq} = 45^o$. The most hydrophobic cases ($\theta_{eq} = 130^o$ and $\theta_{eq} = 120^o$) are not shown because, in those cases, the evaporating nanodroplet desorbs from the substrate, and in the suspended state, neither the contact angle nor the contact radius are defined.

Moreover, we find that the fluctuations in R and θ are concerted. Figure 4 shows a representation of the evaporation process where each scatter point in the plot represents the (R, θ) instantaneous state of the nanodroplet. The size of each scatter point is proportional to the number of water molecules in the nanodroplet at that instant, and each point is colored in a scale from blue to red according to earlier to later times, respectively. In the background of each plot, the isovolumetric contours of the nanodroplets are shown in color as indicated by the color bar. The thin blue lines in the background are the maximum gradient lines. We find that, regardless of hydrophobicity, the fluctuations in R and θ are concerted and approximately follow the isovolumetric contours. The isovolumetric nature of the fluctuations explains, for example, why the fluctuations in R are typically larger for the most hydrophilic cases (e.g., Figure 4A), where the isovolumetric contours are almost parallel to the R-axis.

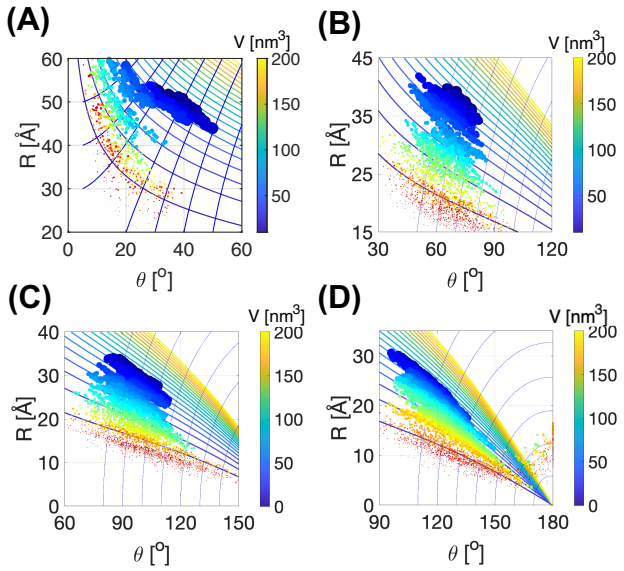

Figure 4. Evaporation of the nanodroplets in the R, θ plane. (A) $\theta_{eq} = 45^o$, (B) $\theta_{eq} = 70^o$, (C) $\theta_{eq} = 90^o$, (D) $\theta_{eq} = 105^o$. The size of each scatter point is proportional to the number of water molecules in the nanodroplet at that instant, each point is colored in a scale from blue to red according to time, and in the background of each plot, the nanodroplet isovolumetric contours are shown in color and the maximum gradient as thin blue lines.

Evaporation Kinetics and Nanodroplet Lifetime. None of the nanodroplets studied conform to the d^2–law predictions ($R^2 \propto -t$). As shown in Figure 5A, R decays linearly over time at a similar rate regardless of the hydrophobicity. The fact that dR/dt is approximately the same for all the cases, however, does not imply that the evaporation rates of the nanodroplets are also the same. Interestingly, when the nanodroplets are suspended, which occurs in the final stages of

evaporation of the most hydrophobic nanodroplets, $R(t)$ follows the classical prediction of the d^2–law, which also applies to free standing nanodroplets (Figure 5B-C).

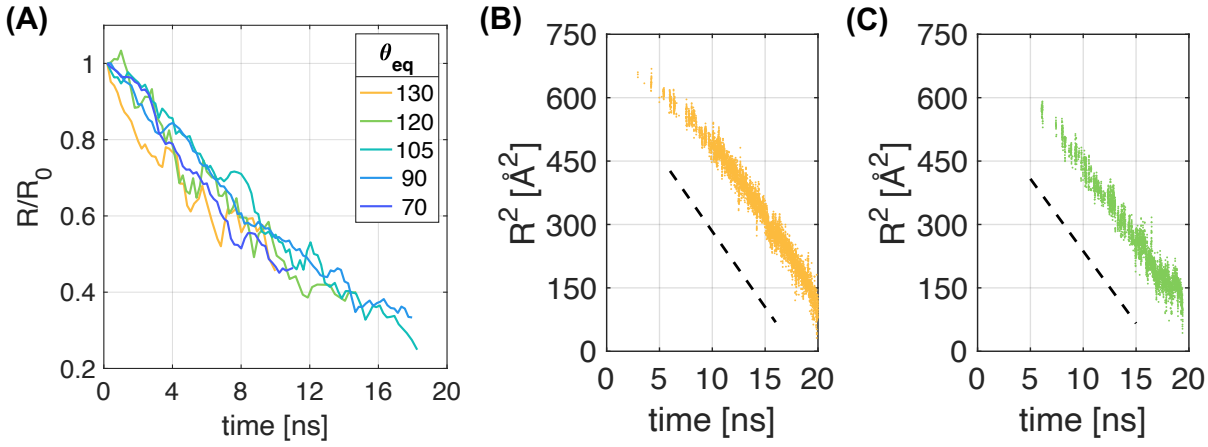

Figure 5. Evolution of the contact radius during evaporation. (A) R is shown normalized by the initial contact radius, R_0, for each case. The curves shown in the plot are the result of performing a moving average with a window size of 0.2 ns on the raw data represented in Figure 2. The most hydrophilic case is not shown, as the evaporation is ultra-fast, in less than 4 ns, and the fluctuations in R are very large (see Figure 2F). (B-C) Evolution of R^2 for hydrophobic nanodroplets ($\theta_{\mathrm{eq}} = 130^o$ and $\theta_{\mathrm{eq}} = 120^o$, respectively) when after they desorb from the substrate and become suspended. The data plotted corresponds to the darker scatter points in Figure 2A-B.

The kinetics of evaporation are significantly different for hydrophilic and hydrophobic nanodroplets. For hydrophilic ones, the evaporation rate is governed by the instantaneous vapor concentration, which, because we are simulating a constant volume system, is just proportional to the number of molecules in the vapor phase: $dn_v/dt \propto -n_v$. Given that $n_v + n_l$ is constant (i.e., a closed system), $dn_v/dt + dn_l/dt = 0$, which implies that $dn_l/dt \propto -n_l$, and n_l decays exponentially with time $n_l(t) \propto e^{-t/t_0}$. This model is in very good agreement with the simulation results of the number of water molecules in the nanodroplet as a function of time (Figure 6A, $\theta_{eq} < 90$), as well as with the evaporation rate, which is maximum initially and decreases exponentially over time (Figure 6B, $\theta_{eq} < 90$). The data shown in Figure 6A, i.e., the number of water molecules in the liquid phase as a function of time, has been calculated according to the criteria described in the *Methods* section. The hydrophobic nanodroplets, on the other hand, exhibit kinetics best described by a stretched exponential:

$$n_l = n_0 e^{-\left(\frac{t}{t_o}\right)^{\alpha}} \quad (1)$$

Where n_0 is the initial number of water molecules in the nanodroplet, t_o is the time scale of the exponential decay, and α is the exponent of the stretched exponential. A key distinction between

the stretched and purely exponential models, is that the evaporation rate becomes a maximum at some intermediate time for the former (Figure 6B, $\theta_{eq} > 90$). We find that the stretching exponent, α, linearly increases with hydrophobicity and becomes unity at $\theta_{eq} \leq 90$ (Figure 6C). The relaxation time scale, t_o, also increases with hydrophobicity, which is consistent with the fact that more hydrophobic nanodroplets evaporate much more slowly.

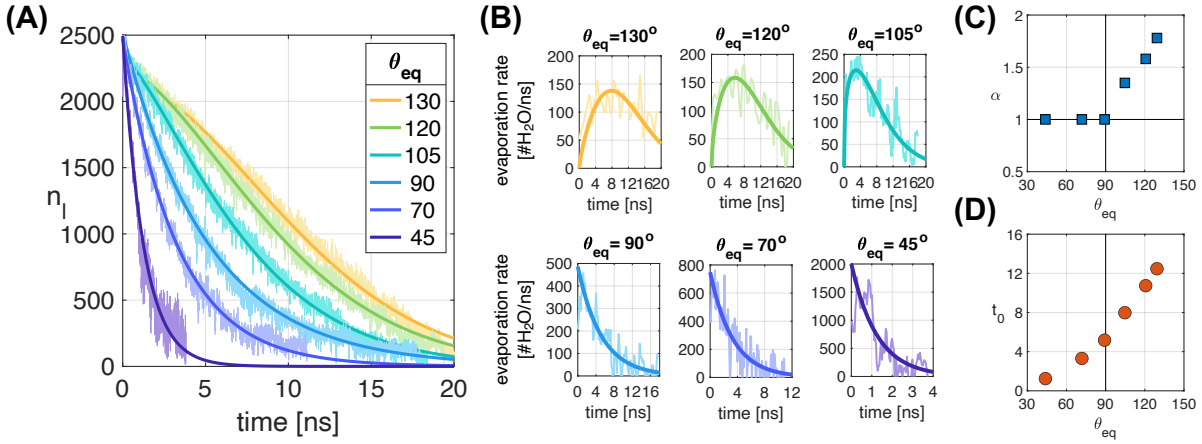

Figure 6. Evaporation kinetics of the nanodroplets. (A) Number of water molecules in the nanodroplets n_l as a function of time. The continuous lines correspond to fits of the model shown in Equation (1) (B) Evaporation rate, in number of water molecules per nanosecond, as a function of time. (C) Parameters of the kinetic model calculated by fitting Equation (1) to the simulation results, as a function of the equilibrium contact angle.

Stretched exponential kinetics are typically associated with complex processes where multiple mechanisms with different relaxation time scales coexist. Therefore, for the hydrophobic nanodroplets, additional factors besides the vapor concentration must be playing a role in the early stages of the evaporation. As shown in Figure 7A, the time that it takes for the nanodroplets to thermalize with the hot substrate monotonically increases as the reduced contact surface area hinders the heat transfer between the substrate and the nanodroplet. We believe that the considerably longer thermalization process in the case of hydrophobic nanodroplets, which is in the same time scale as the evaporation process itself, is the cause of the stretched exponential kinetics. We also find that the duration of the thermalization process is directly correlated to the nanodroplet half-lifetime (Figure 7B). This is in stark contrast with the assumptions of classic theories of evaporation, where the nanodroplet is assumed to be always in thermal equilibrium with the substrate. The longer thermalization times as the hydrophobicity increases, can explain the monotonic increase of the nanodroplets lifetime with hydrophobicity (Figure 7C), which is also at odds with the classical prediction (e.g., see Figure 6 in Ref.[16]).

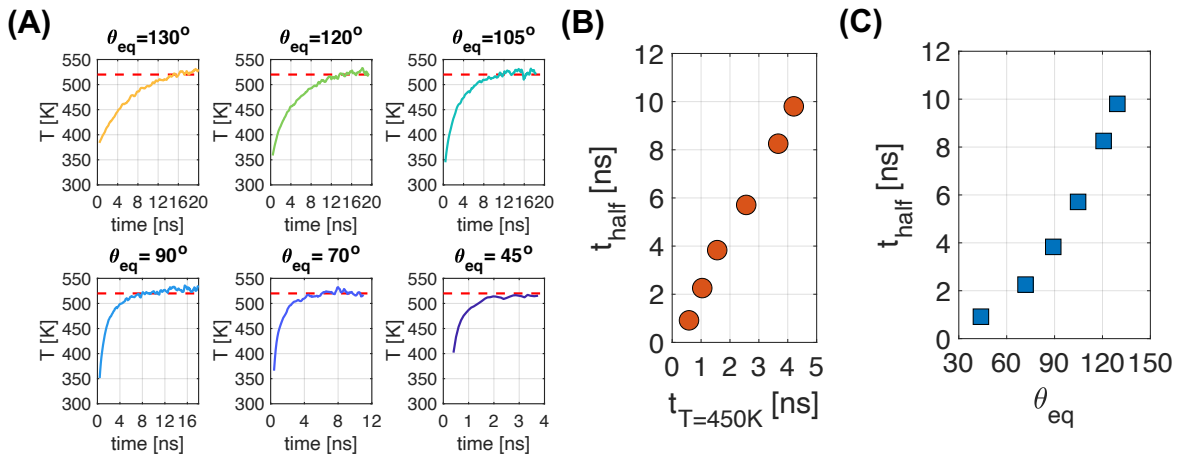

Figure 7. Thermalization of the nanodroplet with the hot substrate. (A) Temperature of the liquid molecules as a function of time. The temperature of the substrate, 520 K, is shown as a red dashed line. (B) Half-lifetime of the evaporating nanodroplets as a function of the thermalization time scale, defined as the time that it takes the nanodroplet to reach a temperature of 450 K. Half-lifetime of the nanodroplets as a function of the equilibrium contact angle.

In addition to the most hydrophilic nanodroplet shown in this paper ($\theta_{\mathrm{eq}} = 45^{\circ}$ which corresponds to a liquid-substrate interaction $\varepsilon_{SO} = 0.30$ kcal/mol), we have simulated nanodroplets with liquid-substrate interactions of 0.32 kcal/mol and 0.34 kcal/mol. We did not include those results in the figures as they significantly depart form the spherical cap morphology of sessile nanodroplets, which is our focus here. In the case where $\varepsilon_{SO} = 0.34$ kcal/mol a thin film of water forms even at room temperature. For $\varepsilon_{SO} = 0.32$ kcal/mol a sessile nanodroplet with θ_{eq} =30° forms at room temperature, but it quickly adopts a thin film morphology during evaporation.

Evaporative flux profile along the nanodroplet surface. To map the evaporative flux profile, we perform an ensemble analysis of the trajectories of each water molecule in the system in which we record the spatial location whenever a molecule transitions from the liquid to the vapor phase (some molecules in the system undergo multiple transitions). To account for the large fluctuations and evolving geometry of the nanodroplet during evaporation we calculate the location of the evaporating molecules in terms of the normalized arclength, $l^{*} \in [0,1]$, which, regardless of nanodroplet size or hydrophobicity, is 0 at the contact line and 1 at the cusp of the nanodroplet. We find that the hydrophilic nanodroplets exhibit a maximum evaporative flux at the contact line, consistent with the observations of hydrophilic macroscopic droplets. Figure 8 shows the evaporative flux as a function of the normalized arclength for all the cases studied here. However, away from the contact line, the flux decays much more gradually than as predicted by

the classical theory, where the flux decays several orders of magnitude over the first ~20% of normalized arclength (see, for example, Figure 4 in Ref [20]). Our results show that the evaporative flux at the cusp of hydrophilic nanodroplets is about 40% of the flux at the contact line. As the substrate becomes more hydrophobic, we observe a transition of the location of the maximum flux away from the contact line, which also agrees with the macroscopic phenomenology. However, in contrast to the theoretical predictions by macroscopic continuum models, where the flux is zero at the contact line and then approximately constant towards the cusp, the evaporative flux in hydrophobic nanodroplets slightly decreases towards the cusp of the nanodroplet. This slight decrease may be explained by the fact that the molecules closer to the hot substrate are more energetic than those at the cusp for hydrophobic nanodroplets.

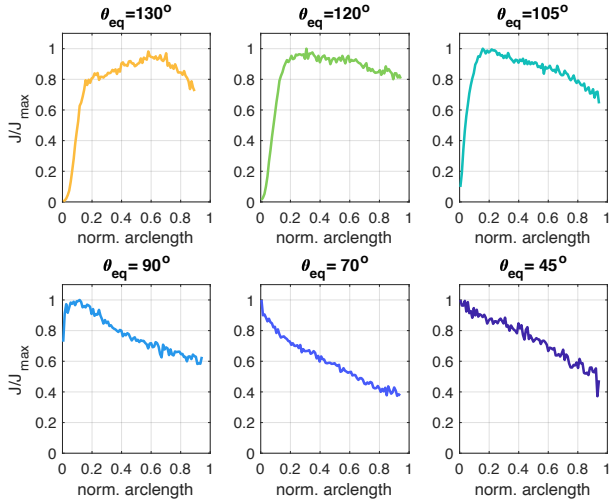

Figure 8. Evaporative flux on the surface of the nanodroplet. The normalized arclength is 0 at the contact line and 1 at the nanodroplet cusp. The flux for the two most hydrophobic cases has been calculated only when the nanodroplets were wetting the substrate.

CONCLUSIONS

We have used molecular dynamics simulations to study how water nanodroplets evaporate on heated substrates with a wide range of hydrophobicities. We found that the evaporative behavior of the nanodroplets is significantly different than that of macroscopic droplets because basic assumptions of the continuum models that hold for macroscopic droplets, are violated at the nanoscale. Specifically, the time scale of evaporation of nanodroplets is of the same order than the diffusive relaxation of the vapor and the thermalization time between the hot substrate and the nanodroplet. As a result, evaporating nanodroplets are not always in thermal equilibrium with the substrate, and the vapor concentration does not reach a steady state. The following evaporative

behavior for sessile water nanodroplets: (i) Nanodroplets do not conform to conventional modes of evaporation (CCR or CCA), but instead exhibit strong dynamic wetting behavior caused, primarily, by thermal effects. As the evaporation progresses and the temperature in the nanodroplets increases, hydrophobic and hydrophilic nanodroplets become more hydrophobic and hydrophilic respectively. The most hydrophobic nanodroplets studied here even desorb from the substrate before fully evaporating. (ii) Evaporating nanodroplets exhibit huge non-equilibrium fluctuations in the contact angle and contact radius, which are concerted and isovolumetric, and which scale with the nanodroplet size as $\Delta \sim N^{-1}$. Fluctuations are negligible in macroscopic droplets. (iii) The evaporation kinetics of nanodroplets do not follow the d^2-*law* observed for macroscopic droplets. Instead, the evaporation of hydrophilic nanodroplets is governed by the instantaneous vapor concentration, which results in an exponential decay of the evaporation rate over time. For hydrophobic nanodroplets, the slow thermalization with the substrate, in the same time scale as the evaporation itself, translates into stretched exponential kinetics, where the maximum evaporation rate occurs at intermediate times. (iv) At odds with the predictions for macroscopic droplets, the evaporative lifetime of nanodroplets is directly proportional to the thermalization time scale, which monotonically increases with hydrophobicity due to the reduced contact area between the nanodroplet and the substrate. (v) The evaporative flux for hydrophilic nanodroplets is maximized at the contact line, similarly to their macroscopic counterparts. However, in contrast to the macroscopic theoretical predictions, the nanodroplets do not exhibit a flux singularity at the contact line, and the flux decays much more slowly from the contact line. For hydrophobic nanodroplets the flux is zero at the contact line and reaches a maximum at the great circle, which also qualitatively agrees with macroscopic expectations. However, the flux does not remain constant from the great circle towards the nanodroplet cusp but instead decays slowly.

The mechanistic understanding gained here into the evaporation of water sessile nanodroplets will be key to interpret future experiments on nanodroplet evaporation and to rationally guide interventions, such as surface treatments to modify the surface hydrophobicity, to modulate evaporation in nanotechnological applications involving water nanodroplet evaporation.

COMPUTATIONAL METHODS

Molecular Dynamics Simulations. All the molecular dynamics (MD) simulations for this study were performed using the program LAMMPS.[41] The water-water interactions are modeled using the TIP4P-Ew force field,[42] a re-parameterization of the standard TIP4P model of water[43]

for use with techniques to account for long-range electrostatics. The SHAKE algorithm is used to constraint the intramolecular bonded interactions in water, and the particle-particle-particle-mesh (PPPM) scheme is used to calculate the long-range coulombic interactions. A Lennard-Jones potential $V_{LJ}(r) = 4\varepsilon[(\sigma/r)^{12} - (\sigma/r)^{6}]$ is used to model the substrate-substrate and substrate-water interactions, where ε and σ are the energy- and length-scale parameters of the potential, respectively. Only the oxygen atoms in water interact with the substrate ($\varepsilon_{sh} = 0$) and the equilibrium distance of the substrate-oxygen interactions is the same as for the oxygen-oxygen interactions ($\sigma_{so} = \sigma_{oo}$). The hydrophobicity of the substrate is therefore controlled by the strength of the substrate-oxygen Lennard-Jones interactions, ε_{so}, relative to the oxygen-oxygen ones, ε_{oo}. In all the simulations we use a timestep of 2 fs and we output the coordinates and velocities of the oxygen and hydrogen atoms every 2 ps for analysis.

In this paper, we present results from two types of simulations on water nanodroplets:

(i) The evaporation of nanodroplets of the same size on substrates heated at the same temperature but with different degrees of hydrophobicity of the solid surfaces. The initial system consists of a semispherical nanodroplet with 2,749 water molecules (~3 nm radius) placed on top of a non-chemically specific substrate 1 nm thick made of atoms arranged in a face centered cubic (FCC) structure. The z-axis is perpendicular to the substrate. The dimensions of the simulation box are 14 x 14 x 15 nm^3 and the system contains a total of 21,501 atoms. A snapshot of the initial configuration of the system and the axisymmetric coordinate system used to analyze the nanodroplets are shown in Figure 9A-B. We simulate the evaporation of nanodroplets on substrates that range from very hydrophobic ($\theta_{\mathrm{eq}} = 130^{o}$) to very hydrophilic ($\theta_{\mathrm{eq}} = 45^{o}$), where θ_{eq} is the equilibrium contact angle of the nanodroplet at room temperature (Figure 9C). We first equilibrate each of the nanodroplets at 300 K for 20 ns. During both equilibration and evaporation stages, the dynamics of the substrate atoms are integrated in the NVT ensemble using a Nose-Hoover thermostat with a damping constant of 100 fs, while the dynamics of the water molecules are integrated in the NVE ensemble to avoid artifacts in the dynamics during the evaporation process due to the thermostat. The equilibrium contact angle, θ_{eq}, is calculated using the last 5 ns of the equilibrium trajectories. After equilibration, we instantaneously increase the temperature of the substrate to 520 K, which is a temperature within the range relevant to droplet evaporation on superheated substrates[36] and of similar value to that used in other previous computational studies.[30, 35] The center of mass of the substrate is constrained during the simulations.

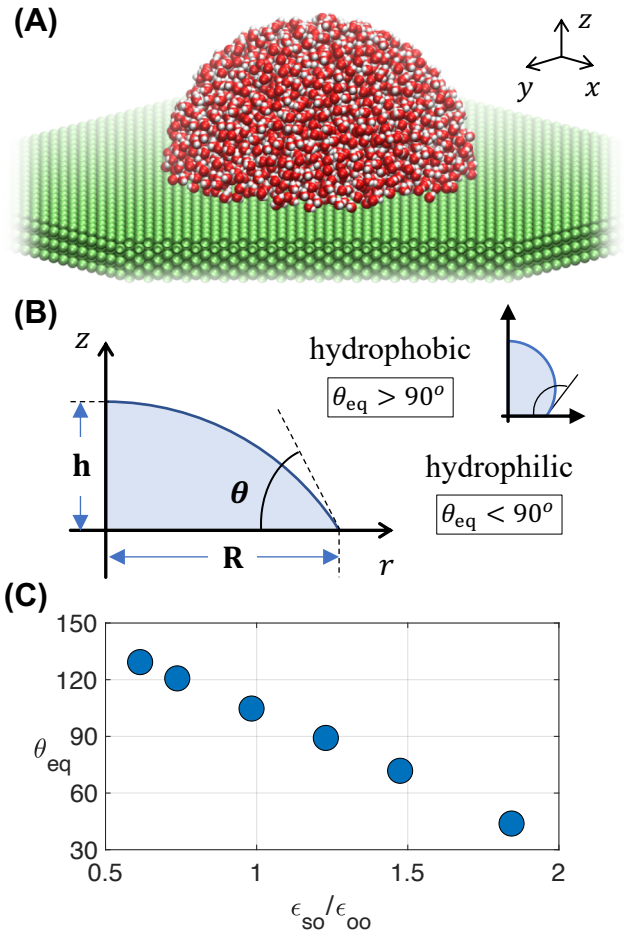

Figure 9. Simulation setup and coordinate system. (A) Snapshot of the initial nanodroplet placed on the substrate. The oxygen atoms are shown in red, the hydrogen atoms in white, and the chemically generic atoms of the substrate are shown in green. (B) Axisymmetric coordinate system used to analyze the nanodroplets, which display a spherical cap geometry at equilibrium and during evaporation. The height of the nanodroplet, h, the contact radius, R, and the contact angle, θ, are shown in bold. According to the contact angle in equilibrium at room temperature, θ_{eq}, we classify the nanodroplets as hydrophilic ($\theta_{eq} < 90$) or hydrophobic ($\theta_{eq} > 90$). (C) Equilibrium contact angle as a function of the relative strength of the substrate-oxygen and oxygen-oxygen interactions, $\varepsilon_{so}/\varepsilon_{oo}$. The error bars are smaller than the symbols.

(ii) The equilibration of nanodroplets of three different sizes (1657, 2763, and 4985 water molecules), on substrates with four different hydrophobicities, heated at three different temperatures (300 K, 350 K, and 400 K). In these simulations, the substrate is still made of atoms arranged in a face centered cubic (FCC) structure, but the substrate is thinner, ~0.7 nm, and smaller 12 x 12 nm^2, to make the simulations less computationally demanding. During these simulations the substrate atoms are tethered to their original positions by harmonic springs. Furthermore, because we are only interested in the equilibrium state of the nanodroplets, the dynamics of all the atoms in the system were integrated in the NVT ensemble. We simulated each system for 20 ns

and calculated the contact angle using the last 10 ns of the trajectory. The nanodroplets were observed to be stable during the time scale of the simulations for all sizes and at all the simulated temperatures.

Analysis of the nanodroplets. Like previous studies, we assume that the nanodroplet is axisymmetric and that it conserves a spherical cap shape during the evaporation process. Both assumptions are reasonably good until the very late stages of evaporation where only a few hundred molecules remain in the liquid phase. To calculate the evolution of the different quantities of interest (e.g., contact angle, contact radius, etc.), we fit the evaporating nanodroplet to a spherical cap using the following protocol. First, we find the center of the droplet in the plane of the substrate and recenter the coordinates with respect to the axisymmetric axis. Once centered, we calculate the polar coordinates (r, z) of all the water molecules in the system and estimate the mass density of water $\rho(r, z)$ (see Figure 1B for an illustration of the coordinate system. Next, we fit a circumference to the boundary points where the density ρ drops to 50% of that of the bulk. From the intersection of the fitted circumference with the plane of the substrate, we can calculate the contact radius, R, the height, h, the contact angle, θ, of the nanodroplet. The molecules within the fitted circumference are considered to be liquid. Those occupying a region of 5 Å beyond the boundary are considered interfacial molecules, and the rest of the water molecules in the system are classified as vapor. It is worth noting that the results of the analysis were not very sensitive to the specific choice of interfacial thickness. All the analysis presented in this paper was carried out using the program MATLAB.

CONFLICT OF INTEREST. The authors declare no conflict of interest

ACKNOWLEDGEMENTS.

We thank the CPIMS program and the Director, Office of Science, Office of Basic Energy Sciences, Chemical Sciences Division of the U.S. Department of Energy under Contract No. DE-AC02-05CH11231. This research used resources of the National Energy Research Scientific Computing Center, a DOE Office of Science User Facility supported by the Office of Science of the U.S. Department of Energy under Contract No. DE-AC02-05CH11231, as well as supercomputing resources of the Institute for Data Science and Computing (IDSC) at the University of Miami.

REFERENCES

1. Kuang, M.; Wang, L.; Song, Y., Controllable Printing Droplets for High-Resolution Patterns. *Advanced Materials* **2014,** *26* (40), 6950-6958.
2. Galliker, P.; Schneider, J.; Eghlidi, H.; Kress, S.; Sandoghdar, V.; Poulikakos, D., Direct printing of nanostructures by electrostatic autofocussing of ink nanodroplets. *Nature Communications* **2012,** *3* (1), 890.
3. Jing, J.; Reed, J.; Huang, J.; Hu, X.; Clarke, V.; Edington, J.; Housman, D.; Anantharaman, T. S.; Huff, E. J.; Mishra, B.; Porter, B.; Shenker, A.; Wolfson, E.; Hiort, C.; Kantor, R.; Aston, C.; Schwartz, D. C., Automated high resolution optical mapping using arrayed, fluid-fixed DNA molecules. *Proceedings of the National Academy of Sciences* **1998,** *95* (14), 8046-8051.
4. Kim, J., Spray cooling heat transfer: The state of the art. *International Journal of Heat and Fluid Flow* **2007,** *28* (4), 753-767.
5. Bar-Cohen, A.; Wang, P.; Rahim, E., Thermal management of high heat flux nanoelectronic chips. *Microgravity Science and Technology* **2007,** *19* (3), 48-52.
6. Brutin, D.; Starov, V., Recent advances in droplet wetting and evaporation. *Chemical Society Reviews* **2018,** *47* (2), 558-585.
7. Kovalchuk, N. M.; Trybala, A.; Starov, V. M., Evaporation of sessile droplets. *Current Opinion in Colloid & Interface Science* **2014,** *19* (4), 336-342.
8. Cazabat, A.-M.; Guéna, G., Evaporation of macroscopic sessile droplets. *Soft Matter* **2010,** *6* (12), 2591-2612.
9. Poulard, C.; Guéna, G.; Cazabat, A. M., Diffusion-driven evaporation of sessile drops. *Journal of Physics: Condensed Matter* **2005,** *17* (49), S4213-S4227.
10. Saxton, M. A.; Whiteley, J. P.; Vella, D.; Oliver, J. M., On thin evaporating drops: When is the d^2-law valid? *Journal of Fluid Mechanics* **2016,** *792*, 134-167.
11. Hu, H.; Larson, R. G., Evaporation of a Sessile Droplet on a Substrate. *The Journal of Physical Chemistry B* **2002,** *106* (6), 1334-1344.
12. Erbil, H. Y.; McHale, G.; Newton, M. I., Drop Evaporation on Solid Surfaces: Constant Contact Angle Mode. *Langmuir* **2002,** *18* (7), 2636-2641.
13. Young, T., III. An essay on the cohesion of fluids. *Philosophical Transactions of the Royal Society of London* **1805,** *95*, 65-87.
14. Varagnolo, S.; Ferraro, D.; Fantinel, P.; Pierno, M.; Mistura, G.; Amati, G.; Biferale, L.; Sbragaglia, M., Stick-Slip Sliding of Water Drops on Chemically Heterogeneous Surfaces. *Physical Review Letters* **2013,** *111* (6), 066101.
15. Yeong, Y. H.; Milionis, A.; Loth, E.; Bayer, I. S., Microscopic Receding Contact Line Dynamics on Pillar and Irregular Superhydrophobic Surfaces. *Scientific Reports* **2015,** *5* (1), 8384.
16. Picknett, R. G.; Bexon, R., The evaporation of sessile or pendant drops in still air. *Journal of Colloid and Interface Science* **1977,** *61* (2), 336-350.
17. Deegan, R. D.; Bakajin, O.; Dupont, T. F.; Huber, G.; Nagel, S. R.; Witten, T. A., Capillary flow as the cause of ring stains from dried liquid drops. *Nature* **1997,** *389* (6653), 827-829.
18. Deegan, R. D.; Bakajin, O.; Dupont, T. F.; Huber, G.; Nagel, S. R.; Witten, T. A., Contact line deposits in an evaporating drop. *Physical Review E* **2000,** *62* (1), 756-765.

19. Jackson, J. D., *Classical electrodynamics*. Third Edition; John Wiley & Sons, Inc.: New York, 1999; pp 75-79.
20. Kadhim, M. A.; Kapur, N.; Summers, J. L.; Thompson, H., Experimental and Theoretical Investigation of Droplet Evaporation on Heated Hydrophilic and Hydrophobic Surfaces. *Langmuir* **2019,** *35* (19), 6256-6266.
21. Nguyen, T. A. H.; Nguyen, A. V.; Hampton, M. A.; Xu, Z. P.; Huang, L.; Rudolph, V., Theoretical and experimental analysis of droplet evaporation on solid surfaces. *Chemical Engineering Science* **2012,** *69* (1), 522-529.
22. Qi, C.; Lei, X.; Zhou, B.; Wang, C.; Zheng, Y., Temperature regulation of the contact angle of water droplets on the solid surfaces. *The Journal of Chemical Physics* **2019,** *150* (23), 234703.
23. Wu, C.-D.; Kuo, L.-M.; Lin, S.-J.; Fang, T.-H.; Hsieh, S.-F., Effects of temperature, size of water droplets, and surface roughness on nanowetting properties investigated using molecular dynamics simulation. *Computational Materials Science* **2012,** *53* (1), 25-30.
24. Montazeri, K.; Abdolhosseini Qomi, M. J.; Won, Y., Solid-like Behaviors Govern Evaporative Transport in Adsorbed Water Nanofilms. *ACS Applied Materials & Interfaces* **2020,** *12* (47), 53416-53424.
25. Zhakhovsky, V. V.; Kryukov, A. P.; Levashov, V. Y.; Shishkova, I. N.; Anisimov, S. I., Mass and heat transfer between evaporation and condensation surfaces: Atomistic simulation and solution of Boltzmann kinetic equation. *Proceedings of the National Academy of Sciences* **2019,** *116* (37), 18209-18217.
26. Varilly, P.; Chandler, D., Water Evaporation: A Transition Path Sampling Study. *The Journal of Physical Chemistry B* **2013,** *117* (5), 1419-1428.
27. Rana, A. S.; Lockerby, D. A.; Sprittles, J. E., Lifetime of a Nanodroplet: Kinetic Effects and Regime Transitions. *Physical Review Letters* **2019,** *123* (15), 154501.
28. Schlesinger, D.; Sellberg, J. A.; Nilsson, A.; Pettersson, L. G. M., Evaporative cooling of microscopic water droplets in vacuo: Molecular dynamics simulations and kinetic gas theory. *The Journal of Chemical Physics* **2016,** *144* (12), 124502.
29. Persad, A. H.; Ward, C. A., Expressions for the Evaporation and Condensation Coefficients in the Hertz-Knudsen Relation. *Chemical Reviews* **2016,** *116* (14), 7727-7767.
30. Montazeri, K.; Hao, S.; Abdolhosseini Qomi, M. J.; Won, Y., Molecular Dynamics Investigation of Liquid and Vapor Interactions Near an Evaporating Interface: A Theoretical Genetics Perspective. *Advanced Theory and Simulations* **2020,** *3* (7), 2000017.
31. Zhang, J.; Huang, H.; Lu, X.-Y., Pinning–Depinning Mechanism of the Contact Line during Evaporation of Nanodroplets on Heated Heterogeneous Surfaces: A Molecular Dynamics Simulation. *Langmuir* **2019,** *35* (19), 6356-6366.
32. Yu, J.-J.; Tang, R.; Li, Y.-R.; Zhang, L.; Wu, C.-M., Molecular Dynamics Simulation of Heat Transport through Solid–Liquid Interface during Argon Droplet Evaporation on Heated Substrates. *Langmuir* **2019,** *35* (6), 2164-2171.
33. Xie, C.; Liu, G.; Wang, M., Evaporation Flux Distribution of Drops on a Hydrophilic or Hydrophobic Flat Surface by Molecular Simulations. *Langmuir* **2016,** *32* (32), 8255-8264.
34. Zhang, J.; Leroy, F.; Müller-Plathe, F., Evaporation of Nanodroplets on Heated Substrates: A Molecular Dynamics Simulation Study. *Langmuir* **2013,** *29* (31), 9770-9782.
35. Zhang, J.; Borg, M. K.; Sefiane, K.; Reese, J. M., Wetting and evaporation of salt-water nanodroplets: A molecular dynamics investigation. *Physical Review E* **2015,** *92* (5), 052403.

36. Putnam, S. A.; Briones, A. M.; Byrd, L. W.; Ervin, J. S.; Hanchak, M. S.; White, A.; Jones, J. G., Microdroplet evaporation on superheated surfaces. *International Journal of Heat and Mass Transfer* **2012,** *55* (21), 5793-5807.
37. Zhang, J.-J.; Huang, H.; Lu, X.-Y., Molecular Dynamics Study of Binary Nanodroplet Evaporation on a Heated Homogeneous Substrate. *Langmuir* **2020,** *36* (13), 3439-3451.
38. Song, J.-W.; Fan, L.-W., Temperature dependence of the contact angle of water: A review of research progress, theoretical understanding, and implications for boiling heat transfer. *Advances in Colloid and Interface Science* **2021,** *288*, 102339.
39. Song, J.-W.; Ma, M.-C.; Fan, L.-W., Understanding the Temperature Dependence of Contact Angles of Water on a Smooth Hydrophobic Surface under Pressurized Conditions: An Experimental Study. *Langmuir* **2020,** *36* (32), 9586-9595.
40. Zhang, J.; Leroy, F.; Müller-Plathe, F., Influence of contact-line curvature on the evaporation of nanodroplets from solid substrates. *Phys Rev Lett* **2014,** *113* (4), 046101.
41. Plimpton, S., Fast Parallel Algorithms for Short-Range Molecular Dynamics. *Journal of Computational Physics* **1995,** *117* (1), 1-19.
42. Horn, H. W.; Swope, W. C.; Pitera, J. W.; Madura, J. D.; Dick, T. J.; Hura, G. L.; Head-Gordon, T., Development of an improved four-site water model for biomolecular simulations: TIP4P-Ew. *The Journal of Chemical Physics* **2004,** *120* (20), 9665-9678.
43. Jorgensen, W. L.; Chandrasekhar, J.; Madura, J. D.; Impey, R. W.; Klein, M. L., Comparison of simple potential functions for simulating liquid water. *The Journal of Chemical Physics* **1983,** *79* (2), 926-935.